Tuning infrared guided-mode resonances with graphene

Domenico de Ceglia, Maria A. Vincenti, Marco Grande, Giuseppe V. Bianco, Giovanni Bruno, Antonella D'Orazio, and Michael Scalora, "Tuning infrared guided-mode resonances with graphene," J. Opt. Soc. Am. B **33**, 426-433 (2016)

https://doi.org/10.1364/JOSAB.33.000426

https://www.osapublishing.org/josab/abstract.cfm?uri=josab-33-3-426

Tuning infrared guided-mode resonances with graphene

DOMENICO DE CEGLIA,[1,*] MARIA A. VINCENTI,[1] MARCO GRANDE,[2] GIUSEPPE V. BIANCO,[3] GIOVANNI BRUNO,[3] ANTONELLA D'ORAZIO,[2] MICHAEL SCALORA[4]

[1] *National Research Council, Charles M. Bowden Laboratory, RDECOM, Redstone Arsenal, Alabama 35898-5000 – USA*
[2] *Dipartimento di Ingegneria Elettrica e dell'Informazione, Politecnico di Bari, Via Re David 200, 70125 Bari, Italy*
[3] *Istituto di Nanotecnologia – CNR-NANOTEC, Via Orabona 4, 70126 Bari, Italy*
[4] *Charles M. Bowden Laboratory, RDECOM, Redstone Arsenal, Alabama 35898-5000 – USA*
**Corresponding author: domenico.deceglia@us.army.mil, domenico.deceglia@gmail.com*

Received XX Month XXXX; revised XX Month, XXXX; accepted XX Month XXXX; posted XX Month XXXX (Doc. ID XXXXX); published XX Month XXXX

We report a strategy to modulate the Fano-like signature of a guided-mode resonance supported by a graphene-based grating. The shape of the resonance is controlled by the amount of damping introduced by graphene. A symmetric-to-asymmetric lineshape transition and a significant narrowing of the linewidth occur at relatively moderate levels of chemical potential. Further increases of the chemical potential lead to a blueshift of the Fano resonance due to the modification of the imaginary part of the conductivity of graphene. Our results are supported by a quasinormal mode analysis of the grating. Using a perturbative approach, we provide analytical expressions for both the resonance wavelength shift and the linewidth modulation induced by changes of the graphene's chemical potential. Electrostatic or electrochemical gating of graphene in the proposed structure provide dynamic control of the Fano-like resonance of the grating, suggesting new opportunities for the design of tunable photonic and optoelectronic devices at infrared wavelengths.

OCIS codes: *(050.0050) Diffraction and gratings; (230.7408) Wavelength filtering devices; (230.5750) Optical devices, resonators; (230.7370) Waveguides.*

http://dx.doi.org/10.1364/AO.99.09999

1. INTRODUCTION

The integration of graphene within photonic resonators promises to lead to tunable and more efficient light matter interactions [1, 2]. While graphene displays a metallic response and supports surface plasmons at mid-infrared and lower frequencies [3], at optical wavelengths it behaves mostly like a lossy dielectric. A single layer of pristine graphene yields single-pass absorption of ~2.3% for visible and near-infrared light, increasing monotonically with the number of graphene layers [4]. The introduction of doping by electrical and/or chemical gating shifts the Fermi energy from the Dirac point and alters the optical response of graphene [5]. For example it was recently demonstrated the ability to chemically control the conductivity of a few-layers graphene film, reaching values of sheet resistance lower than 30 Ω/sq [6]. This opens the possibility to easily tune graphene from the lossy-dielectric to the quasi-metallic region. The resulting modulation capability depends on the strength of light-matter interactions within graphene.

One approach to boost such interactions relies on plasmonics. The plasmonic response may originate from metallic structures [7], from graphene itself [3], or from both systems in hybrid resonators that allow coupling between graphene and metallic plasmons [8]. Another excellent platform that can host enhanced interactions with graphene is based on dielectric photonic cavities. Several structures and devices of this kind have been proposed, including metasurfaces, enhanced sensors, detectors, couplers, and electro-optical light modulators [9-15]. The simplest design probably consists in a Fabry-Pérot cavity that includes graphene. The two surrounding mirrors are usually Bragg reflector multilayers obtained by alternating two dielectric slabs with different indexes of refraction [14, 16-18]. The operational principle of these structures relies on a uniform field enhancement at the graphene location. Total light absorption in mono- or multilayer graphene is obtained in narrow resonance bands when the reflectivity of the two mirrors is properly designed. This phenomenon can be exploited for enhanced third harmonic generation and low-threshold saturable absorption at visible and near-infrared wavelengths, as predicted in defective, asymmetric, one-dimensional photonic crystals that incorporate monolayer graphene [16, 17].

Another promising technique is to exploit guided-mode resonances associated with dielectric gratings [19-21]. A periodically patterned

waveguide supports guided mode resonances. Those resonances might be excited at either normal or oblique incidence thanks to the additional transverse momentum provided by the grating. Although these structures are more sensitive to fabrication accuracy, some of the advantages that these resonators offer over planar, one-dimensional, photonic crystals are reduced thickness and larger local field enhancement. Total light absorption has been theoretically predicted at infrared wavelengths in two-dimensional, graphene-assisted gratings based on silicon [22]. An absorption peak of about 40% (30%) at visible wavelengths for the TE (TM) polarization has been experimentally demonstrated in monolayer-graphene-assisted resonant gratings using a one-dimensional, PMMA grating grown on a tantalum pentoxide guiding film [23]. Coherent perfect absorption has been demonstrated in a similar structure with the aid of a simple mirror that provides constructive interference at the graphene location [24].

In the present work, we explore the possibility to control grating, guided-mode resonances with graphene at telecom wavelengths. We adopt a simple, yet effective physical description of such resonances in terms of quasinormal modes (QNMs) [25]. These modes have complex eigenfrequency and are especially suitable for studying open (or leaky) and lossy cavities [26, 27]. The ability of graphene to alter the QNM complex eigenfrequencies is then assessed by adopting a first-order perturbative approach. We then use the QNMs to describe the grating's guided-mode resonances within the framework of the Fano theory of interference between bright and dark modes [28]. Although this theory was originally developed to study interference effects in solid-state and atomic physics, it may be adapted to many phenomena across different areas of physics and engineering [29]. In the context of guided-mode resonances, the theory predicts the existence of asymmetric lineshape resonances in the transmission and reflection spectra. These spectral features are due to the interference between a continuum (sometimes referred to as direct pathway, bright mode or background, depending on the context) and a discrete state (sometimes referred to as indirect pathway or dark mode). For the resonant grating under investigation, the continuum is the background response of the system in the absence of the periodic dielectric perturbation, whereas the discrete state or set of states are QNMs (sometimes referred to as quasi-guided, leaky modes or quasi-modes) supported by the perturbed waveguide. We explore the possibility to control the Fano-like or guided-mode resonances of such gratings by exploiting the tunability of the graphene conductivity at telecom wavelengths (~1.5μm). Finally, we discuss the design principles of this structure with the aid of both QNMs and Fano theory, and show how to control resonance shape, linewidth and characteristic wavelength of the grating resonances.

2. QUASINORMAL MODE DESCRIPTION OF THE RESONANT GRATING

The geometry of the grating under investigation and the illumination conditions are described in Fig. 1. The structure is similar to that proposed in Ref. [23] with the difference that the principal TE-polarized leaky mode can be excited at normal incidence ($\mathbf{E}_{\text{inc}} = E_{\text{inc}}\hat{\mathbf{x}}$, and $\mathbf{k}_{\text{inc}} = -k_0\hat{\mathbf{z}}$, with k_0 indicating the free-space wavevector) at ~1.55 μm. The high-index guiding layer has a refractive index of n_H = 2.1 (compatible, for example, with Ta_2O_5) and thickness t_H = 150 nm; the low-index, grooved film on top has refractive index n_L = 1.5 (for example, a polymer like PMMA), thickness t_L = 500 nm and periodicity along the y-axis fixed at p = 1 μm (the width of the stripe is equal to a). The SiO_2 substrate has refractive index n_S = 1.5. The graphene plane lies between the high- and the low-index films, with the number of graphene layers equal to N.

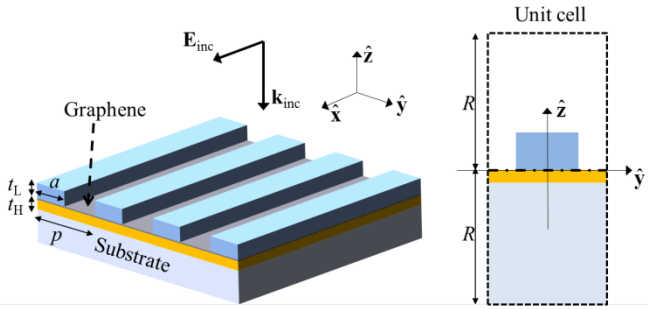

Fig. 1. The grating under investigation and the TE-illumination at normal incidence. On the right, the unit cell of the grating in the yz-plane.

For each graphene monolayer we adopt the closed-form conductivity formula given by Chang et al. [30],

$$\sigma_G = \sigma_0 \left\{ \begin{array}{l} \dfrac{1}{2}\left(\tanh\dfrac{\hbar\omega + 2\mu_c}{4k_B T} + \tanh\dfrac{\hbar\omega - 2\mu_c}{4k_B T} \right) - \\ \dfrac{i}{2\pi}\log\left[\dfrac{\left(\hbar\omega + 2\mu_c\right)^2}{\left(\hbar\omega - 2\mu_c\right)^2 + 4\left(k_B T\right)^2} \right] + \\ \dfrac{4i}{\pi}\dfrac{\mu_c}{\hbar\omega + i\hbar\Gamma} \end{array} \right\}. \qquad (1)$$

The first two terms in Eq. (1) represent the interband response, while the third term arises from intraband transitions. In Eq. (1) k_B is the Boltzmann constant, T the temperature, μ_c is the chemical potential (equal to the Fermi level shift), ω the angular frequency, $\hbar$ is the reduced Planck constant, $\sigma_0 = e^2/(4\hbar)$ is the universal conductivity value for undoped graphene, and e is the elementary electron charge. Henceforth, we consider T = 300 K and we assume an electron relaxation energy Γ= 0.66 meV, corresponding to a relaxation time of ~1.3 ps. The relaxation energy is a measure of the graphene quality. Its impact on the tuning abilities around the resonance wavelength will be discussed in the next section. For simplicity we assume that the optical response of the N-layer graphene may be derived from the conductivity of N graphene monolayers placed in parallel. Hence, the N-layer graphene conductivity is approximated by $\sigma_{NG} \approx N\sigma_G$, thus implying that the graphene electromagnetic response is not significantly altered by the number of graphene layers. This approximation has been demonstrated to be valid at infrared telecom wavelengths, both experimentally and theoretically [31]. In this picture, the in-plane relative permittivity is insensitive to the number of graphene layers N and it reads:

$$\varepsilon_G = \varepsilon_x = \varepsilon_y = 1 + \frac{i\sigma_G}{\omega\varepsilon_0 t_G}, \quad (2)$$

where ε_0 is the vacuum permittivity and $t_G \cong 0.34$ nm is the monolayer graphene thickness. Our calculations are based on the rigorous coupled wave analysis (RCWA) in which the "bulk" model of graphene in Eq. (2) with a finite thickness t_G is adopted. However, RCWA predictions are in excellent agreement with calculations based on the frequency-domain, finite-element method (COMSOL) in which the graphene response is modeled as a surface electric current equal to the discontinuity of the tangential magnetic field and no assumption is made about the graphene thickness [17].

Once the materials are chosen, the spectral position of the grating resonances is very sensitive to the high-index film thickness t_H and the periodicity p. In particular, the phase matching condition to excite a leaky mode is $|\mathbf{k}_{inc}\cdot\hat{\mathbf{y}}+2\pi m/p|=\beta_m$, where $m = 0, \pm1, \pm2,\ldots$ is the grating diffraction order and β_m is the real part of the leaky-mode complex wavenumber. The linewidth of the resonance, which is related to the imaginary part of the complex wavenumber, strongly depends on the grating duty cycle $d = (p - a)/p$.

An effective tool to describe the resonant grating under investigation is based on the theory of QNMs [25, 26]. QNMs are solutions of Maxwell's equations in the absence of sources and with complex eigenfrequency. In particular, in our two-dimensional problem, the QNMs are solutions of the time-harmonic, scalar Helmholtz equation

$$\left[\nabla^2 + \Omega^2 / c_0^2 \varepsilon(\mathbf{r},\Omega)\right]\tilde{E}_x(\mathbf{r},\Omega) = 0, \quad (3)$$

in the unit cell (see Fig. 1), in which $E_x(\mathbf{r},t) = \tilde{E}_x(\mathbf{r},\Omega)\exp(-i\Omega t)$ and $\mathbf{r}=(x,y)$. Periodic boundary conditions are set on the $y = \pm p/2$ edges, i.e., $\tilde{E}_x(\mathbf{r},\Omega) = \tilde{E}_x(\mathbf{r} + p\hat{\mathbf{y}},\Omega)$. Moreover, at the top and bottom edges at $z = \pm R$, radiation boundary conditions are set of the type $\hat{\mathbf{n}}\times\nabla\times\tilde{\mathbf{E}} + i\sqrt{\varepsilon}\Omega/c_0\hat{\mathbf{n}}\times\tilde{\mathbf{E}}\times\hat{\mathbf{n}} = \mathbf{0}$ (with $\hat{\mathbf{n}}$ indicating the unit vector normal to the boundary and pointing outwardly). An alternative way to define outgoing wave conditions is to introduce perfectly matched layers adjacent to the top and bottom edges, as reported for example in Refs. [32, 33]. We have verified that the adoption of either radiation boundary conditions, as defined above, or perfectly matched layers yields almost identical eigensolutions of the problem in Eq. (3). Due to presence of radiation leakage toward the top (air-side, $z > 0$) and bottom (SiO_2-side, $z < 0$) half-spaces, the system is non-conservative and the problem admits eigensolutions $\tilde{E}_{xm}$ corresponding to a discrete set of complex eigenfrequencies $\Omega_m = \omega_m - i\gamma_m$. For each of these QNMs the real part of the eigenfrequency Ω_m represents the spectral position of the corresponding resonance, whereas the imaginary part is its half-width at half-maximum (HWHM) and it accounts for both radiation leakage and material absorption. We note that Eq. (3) is intrinsically nonlinear, since both the permittivity $\varepsilon(\mathbf{r},\Omega)$, which is generally dispersive (e.g., graphene) and the radiation boundary conditions depend on the solution itself. Although analytical approaches are possible for very simple problems, iterative numerical techniques must be generally adopted in order to find the QNMs. In this paper, we use the eigenfrequency finite-element method (COMSOL). If the materials taken into account in the cavity are weakly dispersive, as in the case of graphene at infrared wavelengths, and the initial guess of the eigenfrequency is fairly close to the actual solution, then the problem converges with just a few iterations. Another important aspect of QNMs is that Ω_m is complex hence the time evolution operator is non-Hermitian even in the absence of absorption losses in the cavity. As a consequence, the eigenfields naturally diverge for $|z| \to \infty$ [25], QNMs are difficult to normalize, and useful definitions such as inner product and modal volume are not trivial. However, the completeness of QNMs has been demonstrated in Ref. [26] even for leaky and lossy cavities, and the definition of inner product may be generalized as follows:

$$\left\langle\left\langle \mathbf{f}_m \,|\, \mathbf{f}_m \right\rangle\right\rangle = \frac{1}{c_0^2}\lim_{S\to\infty}\int_S h(\mathbf{r},\Omega_m)\mathbf{f}_m(\mathbf{r})\cdot\mathbf{f}_m(\mathbf{r})d\mathbf{r} + \\ + i\frac{1}{2\Omega_m c_0}\int_\ell \sqrt{\varepsilon(\mathbf{r})}\mathbf{f}_m(\mathbf{r})\cdot\mathbf{f}_m(\mathbf{r})d\mathbf{r}, \quad (4)$$

where $\mathbf{f}_m(\mathbf{r})$ is the eigensolution field corresponding to the eigenfrequency Ω_m, $h(\mathbf{r},\Omega) = (1/2\Omega)\partial\left(\Omega^2\varepsilon(\mathbf{r},\Omega)\right)/\partial\Omega$. The first integral in Eq. (4) is extended on a surface domain S large enough so that the near field of the cavity mode vanishes on its boundary ℓ. In other words, the extension of the surface S in the z direction should be chosen so that only radiation leakage reaches the boundary domain ℓ. Moreover, the permittivity of the materials surrounding the grating (air on the top and SiO_2 on the bottom) are assumed to be dispersion-less in the second integral of Eq. (4). With these precautions in mind, even if both integrals in (4) diverge, their sum is finite and insensitive to the choice of the surface S. QNMs are a powerful tool to predict and describe many effects of the system under investigation. For example, if $\gamma_m << \omega_m$, plane wave excitation of the grating at ω_m *may* produce a resonance in the spectrum. In Fig. 2(a) we map the absorption of the grating, obtained with RCWA, for a normally-incident plane wave tuned around a wavelength of 1.55 μm, and for different values of the grating duty cycle d. Here we assume that the number of graphene layers is $N = 4$ and $\mu_c \to 0$ (undoped graphene). The calculated spectra show an absorption peak whose central wavelength slightly shifts as a function of d. Moreover, the maximum absorption peak (> 0.6) is approached when d is in the range 0.5-0.6, a scenario in which the absorption bandwidth is wider. A simple model of the resonant grating based on the coupled-mode theory [34] indicates that the absorption spectrum near the resonance is proportional to the product of the absorption efficiency (due to graphene) and the radiation efficiency with respect to the input medium (air). Following the technique detailed in Ref. [35], it is possible to evaluate the decay rates due to leakage and absorption losses and demonstrate their strict dependence on the grating duty cycle. As a consequence, the absorption value on-resonance shows a significant sensitivity to the duty cycle d, as illustrated in Fig. 2. We now interpret the observed absorption spectra in terms of resonant

excitation of the QNMs of the structure. In the wavelength range under investigation, we find, by solving the eigenproblem in Eq. (3), that the grating supports two different QNMs, that we call Q_1 and Q_2. The associated eigenfrequencies are $\Omega_{1,2} = \omega_{1,2} - i\gamma_{1,2}$. The characteristic wavelengths of these two modes, $\lambda_{1,2} = 2\pi c_0 / \omega_{1,2}$ (c_0, speed of light in vacuo), are calculated as a function of d and plotted on top of the absorption map in Fig. 2(a). It is clear that the mode Q_1 is resonantly excited by the input plane wave, therefore its wavelength λ_1 shows excellent overlap with the absorption peak. The linewidth of this mode, calculated as $\delta\lambda_1 = 2\pi c_0 \gamma_1 / \omega_1^2$, is plotted in Fig. 2(b) and displays a maximum of ~13 nm for a duty cycle of ~0.6, in agreement with the absorption resonance observed with plane wave excitation. Although not overlapped with the resonant absorption peak, the characteristic wavelength λ_2 of mode Q_2 is not far from λ_1 [see Fig. 2(a)], and its linewidth, $\delta\lambda_2 = 2\pi c_0 \gamma_2 / \omega_2^2$, is similar to $\delta\lambda_1$, even if it decreases monotonically as a function of d [see Fig. 2(b)].

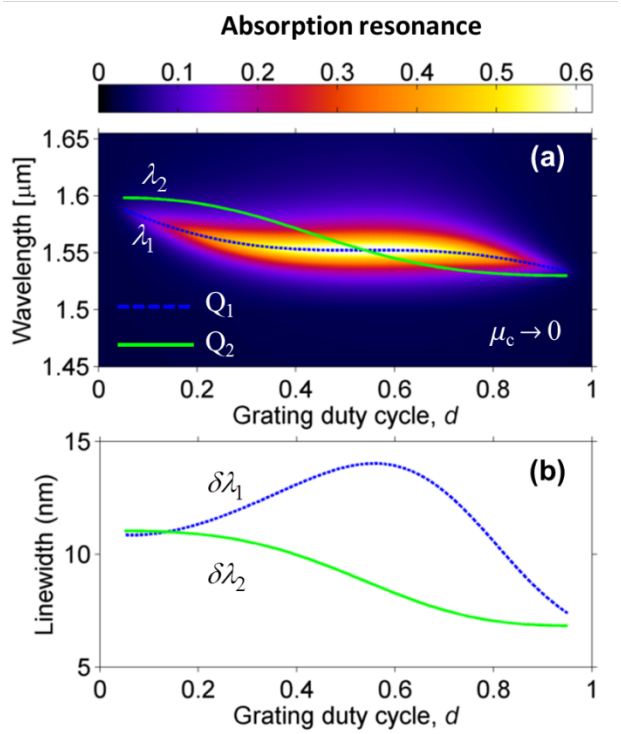

Fig. 2. (a) Color map of the absorption of the grating at normal incidence as a function of wavelength and grating duty cycle d. A four-layer graphene is assumed between the guiding, high-index film and the patterned film on top of it. The dashed, blue line is the wavelength of the dominant QNM Q_1, i.e., $\lambda_1 = 2\pi c_0/\omega_1$, the solid green line is the wavelength of the mode Q_2, $\lambda_2 = 2\pi c_0/\omega_2$. (b) The linewidth of the modes $Q_{1,2}$, $\delta\lambda_{1,2} = 2\pi c_0 \gamma_{1,2}/\omega^2_{1,2}$.

Nevertheless, the excitation of mode Q_2 seems to be forbidden at normal incidence under plane wave illumination, so that no resonant features are associated to this mode in the absorption spectrum. The reason for such dissimilar behavior of the system with respect to modes Q_1 and Q_2 is clarified when the associated eigenfields are inspected. In Figs. 3(a) and 3(b) we plot the electric field's real part of modes Q_1 and Q_2, respectively, for a duty cycle d = 0.5. In both cases, the field overlap with graphene (at z = 0) allows strong interaction and, in principle, light absorption. However, only eigenmode Q_1 [Fig. 3(a)] shows the other decay mechanism, the one related to the radiation losses into the SiO_2 substrate and the air cover. In contrast, the field profile of mode Q_2 is evanescent in the substrate and cover regions, as illustrated in Fig. 3(b). As a consequence, the linewidth $\delta\lambda_2$ of mode Q_2 is merely associated with absorption losses in graphene, whereas the linewidth $\delta\lambda_1$ of Q_1 is also due to radiation leakage therefore it allows for coupling to incident plane waves. Put differently, mode Q_1 is the dominant mode of the system, at least for plane wave excitation at normal incidence. In view of this fact, in the following we will discuss only the effects of the modulation of the graphene chemical potential on such mode.

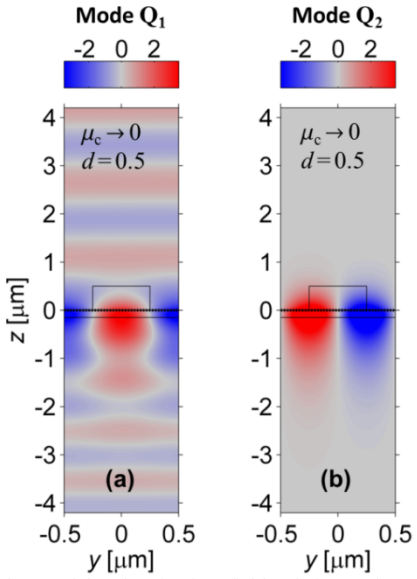

Fig. 3. (a) Real part of the electric eigenfield, relative to the mode Q_1 for a duty cycle d = 0.5. (b) Same as (a) for the eigenfield corresponding to mode Q_2.

3. MODULATING THE FANO RESONANCE OF THE GRATING

In the previous section we assumed undoped graphene ($\mu_c \to 0$ and $\sigma_G \to \sigma_0$) and therefore a scenario of maximized absorption and large resonance bandwidths. In what follows we analyze the behavior of the structure when the graphene chemical potential μ_c is increased. Before discussing the effects on the grating spectra, it is instructive to observe the behavior of the complex permittivity of graphene as a function of μ_c, as illustrated in Fig. 4, for a wavelength (1.55 μm) close to the grating resonance. We stress that the permittivity of graphene shows only slight dispersion across the entire bandwidth of the resonance.

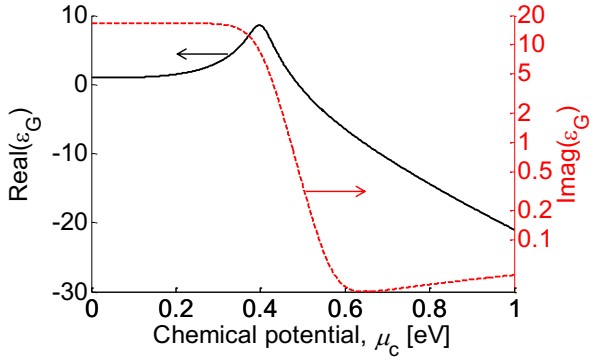

Fig. 4. Graphene permittivity as a function of the chemical potential at a wavelength of 1.55 μm. The logarithmic scale for the imaginary part is used to stress the presence of two plateaus in the graphene response.

The imaginary part of the permittivity decreases significantly when the chemical potential is ~0.5 eV, whereas the real part peaks at $\mu_c \approx 0.4$ eV, crosses zero and drops linearly for increasing values of μ_c. The zero-crossing at $\mu_c \approx 0.4$ eV represents a transition from a lossy-dielectric response to a metallic one. Even if such permittivity changes are remarkable, light interaction with graphene is limited by the inherently small interaction length (a thickness of 1.36 nm for a four-layer graphene film). For this reason, we use a perturbative approach within the theory of QNMs in order to evaluate the impact of modulating μ_c on the Fano resonance wavelength, linewidth and shape. As discussed in Ref. [26], QNMs provide a discrete basis for dealing with perturbations of $\varepsilon(\mathbf{r},\Omega)$ in a leaky and lossy cavity. Initially, we solve the eigenproblem in Eq. (3) for a certain chemical potential value $\mu_c = \mu_{c,0}$. Then we assume the response of the system by considering only the dominant TE-polarized mode $Q_{1,0}$, which has a complex eigenfrequency $\Omega_1(\mu_{c,0}) = \Omega_{1,0}$. A change of μ_c around $\mu_{c,0}$ modulates the graphene permittivity by an amount $\Delta\varepsilon_G(\mu_c) = \varepsilon_G(\mu_c) - \varepsilon_G(\mu_{c,0})$, as shown in Fig. 4. The QNM eigenfrequency is in turn shifted from $\Omega_{1,0}$ to $\Omega_1(\mu_c) = \omega_1(\mu_c) - i\gamma_1(\mu_c)$. We adapt the perturbative expansion for one-dimensional open cavities described in Ref. [26] to our two-dimensional problem in order to estimate $\Omega_1(\mu_c)$. To the first order, the approximation of the perturbed eigenfrequency is given by $\tilde{\Omega}_1(\mu_c) = \Omega_{1,0} + \Delta\Omega_1(\mu_c)$, where

$$\Delta\Omega_1(\mu_c) = -\frac{\Omega_{1,0}}{2}\frac{\tilde{E}_{x1,0}^2\big|_{z=0} Nt_G}{c_0^2\left\langle\left\langle \tilde{E}_{x1,0}\right\rangle\right\rangle}\Delta\varepsilon_G. \qquad (5)$$

In Eq. (5), $\tilde{E}_{x1,0}$ is the *x*-component of the electric field relative to the unperturbed eigenmode $Q_{1,0}$ (obtained for $\mu_c = \mu_{c,0}$) and a uniform field distribution is assumed across the graphene thickness Nt_G. The integration surface in the norm of Eq. (5) is the unit cell illustrated in Fig. 1. The unperturbed eigenmode is calculated for $\mu_{c,0} = 0.4$ eV, within the dielectric-to-metal transition of graphene. Although this choice is arbitrary, we have noticed that the average error $|\tilde{\Omega}_1(\mu_c) - \Omega_1(\mu_c)|$ across the range of interest of μ_c decreases when the initial value , $\mu_{c,0}$, is far from the dielectric and metallic plateau regions of graphene (see Fig. 4), i.e., a good choice is $0.35\text{eV} < \mu_{c,0} < 0.65$ eV. Following this rule, the maximum relative error, calculated as $|\tilde{\Omega}_1 - \Omega_1|/|\Omega_1|$, that we observe for $\mu_c = 1$ eV, is ~ 0.1% on the real part of Ω_1 and ~ 5% on the imaginary part of Ω_1.

We are now able to evaluate the influence of μ_c on the grating resonance. The spectral shift shows a linear dependence on the number of graphene layers *N*. As an example, if *N* = 4 as in the structure of the previous section and the duty cycle is chosen either as *d* = 0.1 or *d* = 0.5, the resonance wavelengths vary as a function of μ_c as illustrated in Fig. 5(a). For both duty cycles the resonance undergoes a deep wavelength shift in the considered range of μ_c; in particular, for the grating with duty cycle *d* = 0.1, the resonance shift is ~18.5 nm while for the grating with *d* = 0.5 the shift is ~16.5 nm. Given the linear dependence of the spectral shift with respect to the number of graphene layers *N*, we predict resonance-wavelength variations of 4 to 5 nm when a monolayer is used instead of the four layers. Our choice of *N* = 4 throughout the paper is only instrumental in providing an illustrative example of the resonance tunability. However, this choice is partly motivated by our recent experimental measurements of the sheet-resistance of chemically-doped, multilayer CVD graphene [6]. These experiments indicate that stacking more than 4-5 parallel layers does not necessarily decrease the sheet-resistance, due to the onset of parasitic series resistances between adjacent layers. In Fig. 5(a), we also highlight the very small difference between the resonance wavelength value $\tilde{\lambda}_1 = 2\pi c_0/\tilde{\omega}_1$ predicted by perturbation theory and the actual QNM wavelength λ_1. We recall that in order to calculate $\tilde{\lambda}_1$ as a function of μ_c it is only necessary to solve once the eigenmode problem (for $\mu_c = \mu_{c,0}$), and then apply the approximation in Eq. (5) in order to evaluate the perturbed eigenfrequencies as μ_c varies. On the other hand, the direct calculation of λ_1 as a function of μ_c requires the solution of the eigenmode problem [Eq. (3)] for each value of μ_c. Therefore, the first approach reduces significantly the computational burden. In Fig. 5(b) we report the linewidth as a function of the chemical potential, for both the considered duty cycles and using both the value of $\delta\lambda_1$, and the perturbation-theory value $\delta\tilde{\lambda}_1$. It is clear that the presence of two plateaus reflects the dielectric-to-metal transition found in the graphene response as a function of μ_c (see Fig. 4). For *d* = 0.1, the linewidth becomes about 20-times smaller as the chemical potential increases, going from ~11nm at low values of μ_c to ~0.5 nm at larger values of μ_c. This also means that the resonance quality factor $\lambda_1/\delta\lambda_1$ increases by a factor of ~20. For *d* = 0.1, the linewidth decreases from ~14 nm to ~4 nm, hence an increase of

quality factor of about 3.5. It is noteworthy that the first-order perturbation theory yields predictions with minimal deviations from the calculations based on the actual QNM eigenfrequencies, even in the presence of such deep modulations of resonance wavelengths and quality factors.

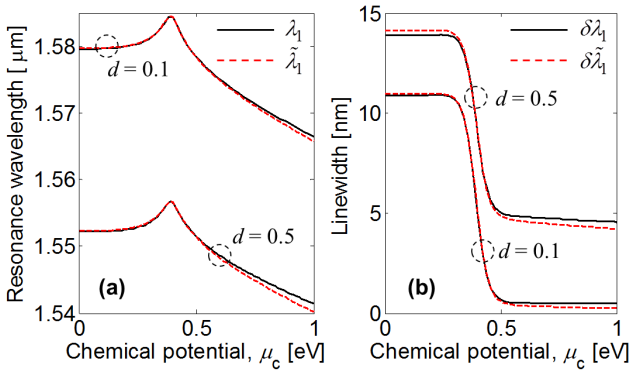

Fig. 5. (a) Resonance wavelength of the grating as a function of chemical potential for two different duty cycle values, $d = 0.1$ and $d = 0.5$. The resonance wavelength is evaluated both by solving the full eigenvalue problem in Eq. (3) (black, solid lines) and by applying the approximation in Eq. (5) derived by the perturbation theory (red, dashed lines). (b) Linewidth of the resonance under the same circumstances described in (a).

A significant aspect of the tunability regards its sensitivity with respect to the intraband electron relaxation energy $\hbar\Gamma$, which is related to the quality of graphene integrated with the grating. If smaller relaxation times are assumed, corresponding to lower graphene quality, the resonance wavelength variations reported in Fig. 5(a) remain virtually unchanged. This is due to the fact that the intraband relaxation energy does not have a large impact on the real part of the graphene permittivity [see Eqs. (1) and (2)]. On the other hand, the imaginary part of the graphene permittivity is very sensitive to $\hbar\Gamma$, therefore less pronounced linewidth variations may be obtained for gratings with lower graphene quality (larger values of $\hbar\Gamma$). In addition to changes of resonance wavelength and linewidth, graphene can also efficiently change the shape of the resonance and the maximum absorption at resonance. In Fig. 6 we report the RCWA-calculated absorption [Figs. 6(a) and 6(b)] and transmission [Figs. 6(c) and 6(d)] maps of the grating as a function of the wavelength and chemical potential μ_c, assuming either $d = 0.1$ or $d = 0.5$. The illumination is at normal incidence and TE-polarized, as illustrated in Fig. 1. The wavelength of the dominant QNM, $\tilde{\lambda}_1$, is superimposed on the spectra, revealing good overlap with the absorption maxima. Not only is the absorption virtually suppressed when $\mu_c > 0.4$ eV, but also the shape of the resonance undergoes a remarkable variation as a function of the chemical potential. We identify two distinct regimes, corresponding to the two plateaus found in the imaginary part of the graphene permittivity, as shown in Fig. 4. In the lossy-dielectric regime ($\mu_c < 0.4$ eV), the resonance shape is symmetric or Lorentzian-like, while in the low-loss, metallic regime ($\mu_c > 0.4$ eV) the shape becomes asymmetric or Fano-like. This strong variation is strictly related to the behavior of the imaginary part of the graphene permittivity as a function of μ_c. In order to assess the ability of the graphene-assisted grating to tune the shape of the resonance, we resort to an analytic model for the guided-mode resonance based on the Fano theory. In particular, we assume that the transmission spectrum of the structure obeys to the generalized Fano formula described in [36] for lossy systems,

$$T(\omega) = T_{bg}(\omega)\frac{(w+q)^2 + b}{w^2 + 1} \qquad (6)$$

where q is the symmetry or shape factor, b is the modulation damping parameter and the reduced frequency is defined as $w = (\omega - \omega_1)/\gamma_1$. Following the procedure described in Ref. [35], the transmission of the Fabry-Pérot background, $T_{bg}(\omega)$, is computed via transfer matrix as the transmission of an equivalent unpatterned structure with the top grating layer replaced by an effective planar film of refractive index $n_{eff} = \sqrt{d + (1-d)n_L^2}$. The Fano profile described by Eq. (6) is generally asymmetric, in the sense that the transmission undergoes an abrupt variation from a low to a high state near the resonance. In the damping-free case (i.e., $b = 0$), symmetric spectral features correspond usually to the antiresonance that one obtains for $q = 0$ and to the Lorentz-like resonance associated with large values of the shape factor q. However, in the model adopted here, the shape is influenced not only by the parameter q but also by the modulation damping parameter b. In fact, the presence of b prevents the transmission from completely vanishing. More specifically, a large value of b induces a low contrast in the resonance and leads to a small ratio between minimum and maximum transmission near the resonance.

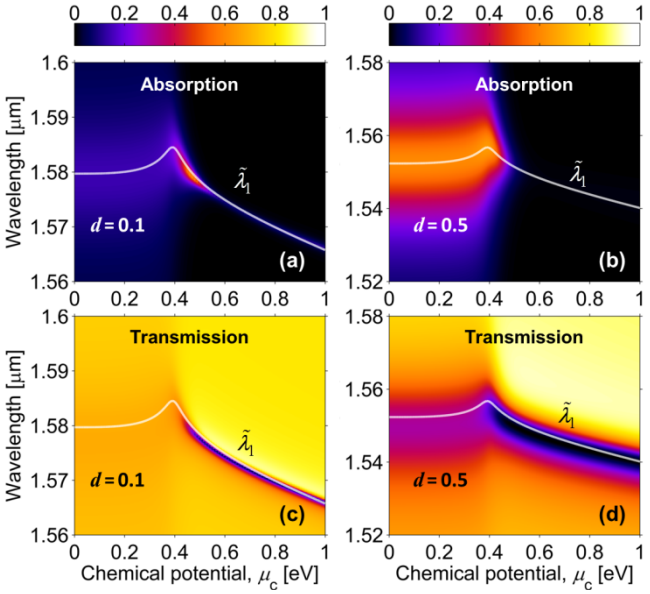

Fig. 6. (a) Absorption and (c) transmission of the grating as a function of chemical potential and input wavelength for TE-polarized plane waves at normal incidence, assuming $d = 0.1$. The white line is the characteristic wavelength of the perturbed QNM Q_1, evaluated via Eq. (5). (b) and (d) Same as (a) and (c), respectively, with $d = 0.5$.

We fitted the grating RCWA-transmission at normal incidence with the generalized Fano formula by using the QNM eigenfrequency $\Omega_1 = \omega_1 - i\gamma_1$ in order to define the reduced frequency w in Eq. (6). Hence, the fitting was performed with the two parameters q and b. Two structures with different duty cycles (d = 0.1 in the first and d = 0.5 in the second grating) and two values of chemical potential (μ_c = 0.1 eV and μ_c = 0.6 eV) were considered in the calculations, assuming again a number of graphene layers N = 4. The retrieved Fano parameters are shown in Table 1. The comparison between the analytic Fano formula with parameters as in Table 1 and the corresponding RCWA-spectra is shown in Fig. 7.

Table 1. Eigenfrequencies and Fano fitting parameters *q* and *b*, for four different scenarios corresponding to the combinations of duty cycle and chemical potential specified in the first two columns.

d	μ_c [eV]	ω_1 [THz]	γ_1 [THz]	q	b
0.1	0.1	1192	8.217	–0.0173	0.9072
0.1	0.6	1197	0.3933	–0.3500	0.0100
0.5	0.1	1213	10.84	–0.1148	0.4119
0.5	0.6	1217	3.779	–0.3328	0.0069

We are now able to conclude that besides modulating the complex eigenfrequency of the structure, graphene also induces changes in shape and contrast of the Fano resonance. For example, the grating with duty cycle d = 0.1 shows only a shallow and symmetric (Lorentz-like) resonance at a low value of chemical potential (μ_c = 0.1 eV); however, when μ_c is increased to 0.6 eV the asymmetry parameter q increases by a factor of 200 and the damping parameter b decreases by a factor of 900. Although less pronounced, similar variations of shape and damping are observable for the grating with duty cycle d = 0.5 under the same variation of chemical potential.

4. CONCLUSIONS

We have shown that the introduction of graphene in dielectric gratings operating at infrared telecom wavelengths may pave the way for the development of tunable resonators and absorbers. The guided-mode resonances of the structure were analyzed through the quasinormal mode theory. The ability of graphene to modulate the complex eigenfrequency of such modes was investigated by means of a first-order perturbative approach. The agreement of this approach with full-wave simulations has been verified in a wide range of graphene doping levels. The modal analysis has also been instrumental in describing resonant effects using a generalized Fano formula. We find that by increasing the graphene chemical potential one is able not only to reduce the resonance linewidth and shift the resonance wavelength, but also to significantly alter the resonance shape. In particular, we identify two distinct operational regimes. Below a certain gating threshold, the structure displays a symmetric absorption resonance whose characteristic wavelength and linewidth are virtually insensitive to the graphene chemical potential. Above this threshold, the real part of the graphene conductivity decreases significantly so that the resonance becomes narrower and asymmetric. In this regime, one can exploit changes of the imaginary part of the graphene conductivity in order to modulate the resonance wavelength.

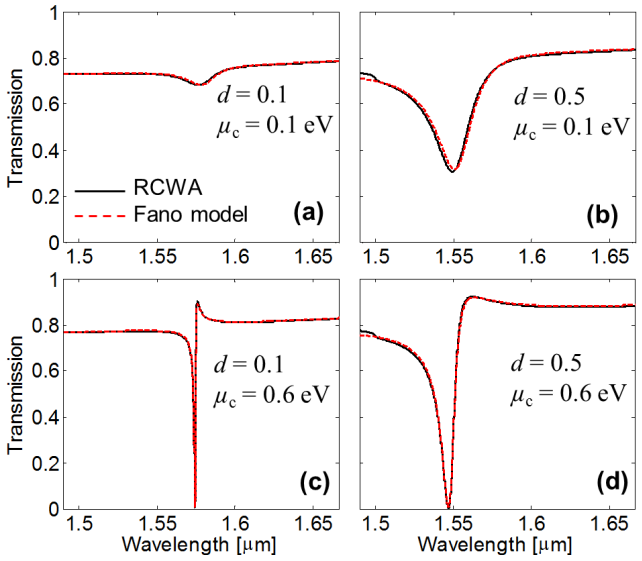

Fig. 7. (a) Transmission of the grating at normal incidence for TE-polarization as a function of wavelength, assuming d = 0.1 and μ_c = 0.1 eV. The black line is the RCWA spectrum, while the red, dashed line is the Fano profile obtained from Eq. 6 with parameters taken from Table I. (b) Same as (a) with d = 0.5 and μ_c = 0.1 eV. (c) Same as (a) with μ_c increased from 0.1 to 0.6 eV. (d) Same as (b) with μ_c increased from 0.1 to 0.6 eV.

Acknowledgments. This research was performed while D. de Ceglia and M. A. Vincenti held a National Research Council Research Associateship award at the U.S. Army AMRDEC. M. Grande thanks the U.S. Army International Technology Center Atlantic for financial support (W911NF-13-1-0434). G. V. Bianco and G. Bruno acknowledge funding from the National Laboratory Sens&Micro LAB Project (POFESR 2007-2013, code number 15) funded by Apulia Region.

REFERENCES

1. F. Bonaccorso, Z. Sun, T. Hasan, and A. C. Ferrari, "Graphene photonics and optoelectronics," Nat Photon **4**, 611-622 (2010).
2. Q. Bao and K. P. Loh, "Graphene Photonics, Plasmonics, and Broadband Optoelectronic Devices," ACS nano **6**, 3677-3694 (2012).
3. A. N. Grigorenko, M. Polini, and K. S. Novoselov, "Graphene plasmonics," Nat Photon **6**, 749-758 (2012).
4. R. R. Nair, P. Blake, A. N. Grigorenko, K. S. Novoselov, T. J. Booth, T. Stauber, N. M. R. Peres, and A. K. Geim, "Fine Structure Constant Defines Visual Transparency of Graphene," Science **320**, 1308-1308 (2008).
5. F. Wang, Y. Zhang, C. Tian, C. Girit, A. Zettl, M. Crommie, and Y. R. Shen, "Gate-Variable Optical Transitions in Graphene," Science **320**, 206-209 (2008).
6. M. Grande, G. V. Bianco, M. A. Vincenti, D. de Ceglia, P. Capezzuto, M. Scalora, A. D'Orazio, and G. Bruno, "Optically transparent microwave

polarizer based on quasi-metallic graphene," Scientific Reports **accepted**(2015).
7. Y. Yao, M. A. Kats, P. Genevet, N. Yu, Y. Song, J. Kong, and F. Capasso, "Broad Electrical Tuning of Graphene-Loaded Plasmonic Antennas," Nano Letters **13**, 1257-1264 (2013).
8. D. A. Smirnova, A. E. Miroshnichenko, Y. S. Kivshar, and A. B. Khanikaev, "Tunable nonlinear graphene metasurfaces," Physical Review B **92**, 161406 (2015).
9. A. Majumdar, K. Jonghwan, J. Vuckovic, and W. Feng, "Graphene for Tunable Nanophotonic Resonators," Selected Topics in Quantum Electronics, IEEE Journal of **20**, 68-71 (2014).
10. T. Mueller, F. Xia, and P. Avouris, "Graphene photodetectors for high-speed optical communications," Nat Photon **4**, 297-301 (2010).
11. A. Locatelli, A.-D. Capobianco, M. Midrio, S. Boscolo, and C. De Angelis, "Graphene-assisted control of coupling between optical waveguides," Opt. Express **20**, 28479-28484 (2012).
12. V. Sorianello, M. Midrio, and M. Romagnoli, "Design optimization of single and double layer Graphene phase modulators in SOI," Opt. Express **23**, 6478-6490 (2015).
13. M. Midrio, S. Boscolo, M. Moresco, M. Romagnoli, C. De Angelis, A. Locatelli, and A.-D. Capobianco, "Graphene–assisted critically–coupled optical ring modulator," Opt. Express **20**, 23144-23155 (2012).
14. R. Yu, V. Pruneri, and F. J. García de Abajo, "Resonant Visible Light Modulation with Graphene," ACS Photonics **2**, 550-558 (2015).
15. C. Wu, N. Arju, G. Kelp, J. A. Fan, J. Dominguez, E. Gonzales, E. Tutuc, I. Brener, and G. Shvets, "Spectrally selective chiral silicon metasurfaces based on infrared Fano resonances," Nat Commun **5**(2014).
16. M. A. Vincenti, D. de Ceglia, M. Grande, A. D'Orazio, and M. Scalora, "Nonlinear control of absorption in one-dimensional photonic crystal with graphene-based defect," Optics Letters **38**, 3550-3553 (2013).
17. M. A. Vincenti, D. de Ceglia, M. Grande, A. D'Orazio, and M. Scalora, "Third-harmonic generation in one-dimensional photonic crystal with graphene-based defect," Physical Review B **89**, 165139 (2014).
18. M. Furchi, A. Urich, A. Pospischil, G. Lilley, K. Unterrainer, H. Detz, P. Klang, A. M. Andrews, W. Schrenk, G. Strasser, and T. Mueller, "Microcavity-Integrated Graphene Photodetector," Nano Letters **12**, 2773-2777 (2012).
19. R. Magnusson and S. S. Wang, "New principle for optical filters," Applied Physics Letters **61**, 1022-1024 (1992).
20. A. Hessel and A. A. Oliner, "A New Theory of Wood's Anomalies on Optical Gratings," Appl. Opt. **4**, 1275-1297 (1965).
21. S. Fan, W. Suh, and J. D. Joannopoulos, "Temporal coupled-mode theory for the Fano resonance in optical resonators," J. Opt. Soc. Am. A **20**, 569-572 (2003).
22. J. R. Piper and S. Fan, "Total Absorption in a Graphene Monolayer in the Optical Regime by Critical Coupling with a Photonic Crystal Guided Resonance," ACS Photonics **1**, 347-353 (2014).
23. M. Grande, M. A. Vincenti, T. Stomeo, G. V. Bianco, D. de Ceglia, N. Aközbek, V. Petruzzelli, G. Bruno, M. De Vittorio, M. Scalora, and A. D'Orazio, "Graphene-based absorber exploiting guided mode resonances in one-dimensional gratings," Opt. Express **22**, 31511-31519 (2014).
24. M. Grande, M. A. Vincenti, T. Stomeo, G. V. Bianco, D. de Ceglia, N. Aközbek, V. Petruzzelli, G. Bruno, M. De Vittorio, M. Scalora, and A. D'Orazio, "Graphene-based perfect optical absorbers harnessing guided mode resonances," Opt. Express **23**, 21032-21042 (2015).
25. E. S. C. Ching, P. T. Leung, A. Maassen van den Brink, W. M. Suen, S. S. Tong, and K. Young, "Quasinormal-mode expansion for waves in open systems," Reviews of Modern Physics **70**, 1545-1554 (1998).
26. P. T. Leung, S. Y. Liu, and K. Young, "Completeness and orthogonality of quasinormal modes in leaky optical cavities," Physical Review A **49**, 3057-3067 (1994).
27. A. Settimi, S. Severini, N. Mattiucci, C. Sibilia, M. Centini, G. D'Aguanno, M. Bertolotti, M. Scalora, M. Bloemer, and C. M. Bowden, "Quasinormal-mode description of waves in one-dimensional photonic crystals," Physical Review E **68**, 026614 (2003).
28. U. Fano, "Effects of Configuration Interaction on Intensities and Phase Shifts," Physical Review **124**, 1866-1878 (1961).
29. A. E. Miroshnichenko, S. Flach, and Y. S. Kivshar, "Fano resonances in nanoscale structures," Reviews of Modern Physics **82**, 2257-2298 (2010).
30. Y.-C. Chang, C.-H. Liu, C.-H. Liu, Z. Zhong, and T. B. Norris, "Extracting the complex optical conductivity of mono- and bilayer graphene by ellipsometry," Applied Physics Letters **104**, 261909 (2014).
31. K. F. Mak, M. Y. Sfeir, J. A. Misewich, and T. F. Heinz, "The evolution of electronic structure in few-layer graphene revealed by optical spectroscopy," Proceedings of the National Academy of Sciences **107**, 14999-15004 (2010).
32. C. Sauvan, J. P. Hugonin, I. S. Maksymov, and P. Lalanne, "Theory of the Spontaneous Optical Emission of Nanosize Photonic and Plasmon Resonators," Physical Review Letters **110**, 237401 (2013).
33. B. Vial, F. Zolla, A. Nicolet, and M. Commandré, "Quasimodal expansion of electromagnetic fields in open two-dimensional structures," Physical Review A **89**, 023829 (2014).
34. H. A. Haus, *Waves and fields in optoelectronics* (Prentice Hall, Incorporated, 1984).
35. J. W. Yoon and R. Magnusson, "Fano resonance formula for lossy two-port systems," Opt. Express **21**, 17751-17759 (2013).
36. B. Gallinet and O. J. F. Martin, "\textit{Ab initio} theory of Fano resonances in plasmonic nanostructures and metamaterials," Physical Review B **83**, 235427 (2011).